Journal of Materials Chemistry C

Accepted Manuscript

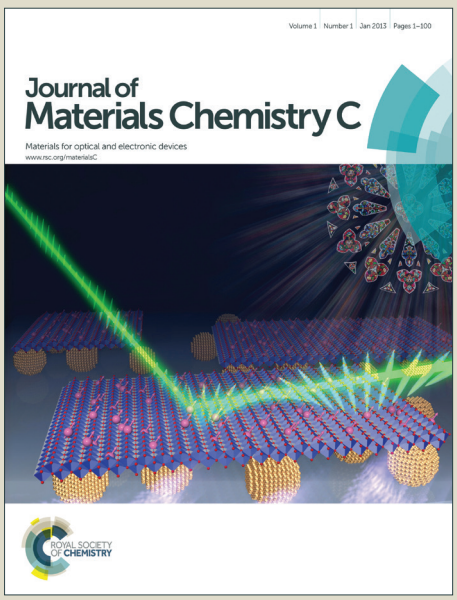

ROYAL SOCIETY OF CHEMISTRY

www.rsc.org/materialsC

Structural and luminescent properties of red-emitting rare earth antimonates Eu^{3+}-doped ternary R_3SbO_7 (R=La, Gd, Y)

Jing Wang,[a] Yu cheng,[a] Yanlin Huang,[a*] Peiqing Cai,[b] Sun Il Kim,[b] Hyo Jin Seo[b*]

[a] *College of Chemistry, Chemical Engineering and Materials Science, Soochow University, Suzhou 215123, China*

[b] *Department of Physics and Center for Marine-Integrated Biomedical Technology, Pukyong National University, Busan 608-737, Republic of Korea*

Abstract

The red-emitting rare earth antimonates of Eu^{3+}-doped R_3SbO_7 (R=La, Gd, Y) were prepared by the high-temperature solid-state reaction. The crystal-phase formations were verified by X-ray powder diffraction (XRD) and structural refinements. The luminescence properties such as photoluminescence (PL) excitation and emission spectra, fluorescence decay curves, absolute luminescence quantum efficiency (QE), CIE color coordinates and the dependence of luminescence intensity on doping level were investigated. The luminescence QE, CIE color coordinations, and the spectrum characteristics of Eu^{3+} ions have the strong dependences on both R (La, Gd, Y) cations and Eu^{3+} doping levels. $^5D_0 \rightarrow {}^7F_4$ emission peak at 710 nm was the dominated

* Corresponding authors E-mail address: hjseo@pknu.ac.kr (Hyo Jin Seo); and huang@suda.edu.cn (Yanlin Huang)

transition in Eu^{3+}-doped La_3SbO_7, while $^5D_0 \rightarrow {}^7F_0$ at 580 nm presents the strongest transition intensity in Eu^{3+}-doped Y_3SbO_7. The luminescence properties were discussed on the base of the crystal structure. Different Eu^{3+} luminescence centers such as isolated centers, the pair broadening, and cluster centers were discussed on the dependence of the lifetime values on Eu^{3+}-concentration. The luminescence QE of La_3SbO_7:0.4Eu^{3+} can reach 63.8 % under the excitation of UV light at room temperature. The potential application as red-emitting phosphor for solid state lighting can be suggested.

Keywords: Rare earth ions; Luminescence; Eu^{3+}; Optical materials and properties

1. Introduction

During the past decades, rare-earth (RE) ions doped materials have attracted extensive attention due to the rich luminescent properties and the potential applications in laser materials, flat panel display, cathode ray tubes, up-conversion materials, white light emitting diodes (W-LEDs), X-ray scintillators and so on.[1-7]

Europium ion (Eu^{3+}) is one of the most interesting RE activators. On the base of the emission spectra, Eu^{3+} ions have special luminescence properties.[8,9] As an important activator, Eu^{3+} ions have pure red emission transitions with a series of sharp lines arising from the excited state $^5D_0$ to the lower energy state $^7F_{0-6}$. $^5D_0 \rightarrow {}^7F_2$ electric dipole (ED) transitions around 612 nm are highly hypersensitive, which is highly sensitive to the symmetry of the Eu^{3+} sites in the lattices. $^5D_0 \rightarrow {}^7F_1$ magnetic dipole (MD) transitions around 590 nm are allowed, which is insensitive to the symmetric environment of the rare-earth ion. The $^7F_0$ and $^5D_0$ levels are non-degenerant and the spectra associated with transitions between them should contain as many lines as the number of nonequivalent sites.[10] Eu^{3+} The luminescence decay time of the emitting $^5D_0$ level (ms) is longer.[11] Therefore, Eu^{3+} ions have been widely investigated for applications as phosphors, electroluminescent devices, optical amplifiers and density optical storage.[12,13] The important factor that affects the emission of the Eu^{3+} is the environment in the host lattices. A small difference of host structure can have also an important influence on the luminescent properties of Eu^{3+} ions-doped phosphors.

In this work, we selected the ternary rare earth antimonates R_3SbO_7 to accommodate Eu^{3+} ions and investigate the red luminescence properties with different cations *R*=La, Gd, and Y. The hosts belong to the ternary rare earth compounds with a general formula R_3MO_7 (*M*=Sb, Ta, Re, Ru, etc.), which have high chemical stability, lattice stiffness, thermal stability, etc. This kind of structure allows a wide variety of chemical substitutions at the *R* and *M* sites (3+ and 4+ or 2+ and 5+ combinations of valence, as well as oxygen vacancies). *R* sites can accommodate all the rare

earth ions together with yttrium; have an ordered, defect-fluorite superstructure. The compounds are supposed to derive from fluorite structure $M_4^{4+}O_8$ as the following manner: four tetravalent ions metal M^{4+} are replaced by three trivalent ions (R^{3+}) and one pentavalent ion (Sb), one oxide vacancy is formed per fluorite cell.[14] Due to the significant differences in radii between the R^{3+} and M^{5+} ions, cation ordering occurs on the metal sites and the oxide-vacancy orders on the anion sites.[15] For the antimonate compounds R_3SbO_7, the crystal structures have been investigated;[16] however, the applications are limited. By now, only magnetic and thermal properties have been reported for R_3SbO_7 (R= rare earths) compounds.[15]

In this paper, Eu^{3+}-doped antimonates R_3SbO_7 (R=La, Gd, Y) were synthesized by the conventional high temperature solid-state reaction to develop red-emitting phosphors. In R_3SbO_7 (R=La, Gd, Y) the doping level of Eu^{3+} ions was decided to be 5-100 mol % in order to investigate the evolution of emission spectra as function of the concentration. The phosphors were characterized by X-ray diffraction (XRD), SEM, the photoluminescence (PL) excitation and emission spectra. The luminescence characteristics were discussed on the base of its special crystal structure. The lifetimes of the Eu^{3+} doped compounds as function of activator ions concentration were investigated. The luminescence mechanism was discussed on the relationship between the crystal structure and luminescence properties of Eu^{3+} ions.

2. Experimental

Polycrystalline rare earth antimonate samples $R_{3-3x}Eu_{3x}SbO_7$ (R=La, Gd, Y, x=0.05-1.0) were synthesized via the solid-state reaction. The starting material was a stoichiometric mixture of reagent grade R_2O_3 (R=La, Gd, Y, and Eu) and Sb_2O_3 (≥ 99.9 % Aldrich, or Alfa Aesar). The starting materials were intimately ground and heated in air with a stepwise method over a period of time reaching the highest temperature of 1550 ^oC. Firstly, the mixture was heated up to 1250 °C and kept at this temperature for 3-5 h. Secondly, the obtained powder was thoroughly mixed in acetone and then heated at 1450 °C for 5 h in air. After that the samples were mixed and were finally heated at 1550 °C for 8 h in air atmosphare. The phase purity of the final products was checked by powder X-ray diffraction (XRD).

The XRD pattern was collected on a Rigaku D/Max diffractometer operating at 40 kV, 30 mA with Bragg–Brentano geometry using Cu-Kα radiation (λ=1.5405 Å) and analyzed by using Jade-5.0 software Program. Structural refinements of X/ray diffractogram were made using the GSAS (general structure analysis system) program.[17] The microstructure morphology of the samples was investigated using scanning electron microscopy (JSM-6700F, JEOL Ltd., Tokyo, Japan). Photoluminescence excitation spectra and luminescence spectra were recorded on a Perkin-Elmer LS-50B luminescence spectrometer with Monk–Gillieson type monochrometers and a xenon discharge lamp used as excitation source. Photoluminescence quantum efficiency, i.e., internal QE, was measured by an Absolute Photoluminescence Quantum Yield Measurement System (Hamamats u-Photonics C9920-02). A 150 W CW Xenon light is applied as the excitation source. This spectrometer is equipped an integrating sphere coated with Lambertian reflector, an

ultra-high sensitivity Photonic multichannel analyzer (PMA-12) and a computer with a photoluminescence measurement software.

For the measurements of luminescence decay curves, the samples were excited by a pulsed Nd:YAG laser at 266 nm (Spectron Laser System SL802G). The luminescence was dispersed by the 75 cm monochromator (Acton Research Corp. Pro-750) and multiplied by the PMT (Hamamatsu R928). The data was displayed and recorded with the LeCloy 9301 digital storage oscilloscope.

3. Results

3.1 *The phase formation and crystal structure*

Eu^{3+}-doped R_3SbO_7 samples were checked by XRD measurements. Fig. 1 shows the representative XRD patterns of Eu^{3+}-doped Y_3SbO_7 and Gd_3SbO_7 at room temperature. All patterns are compared with the refered standard card PDF#2 No.24-0420 (Gd_3SbO_7) selected in the International Centre for Diffraction Data (ICDD) database. No other impurities could be found. It is obvious that the XRD patterns of Y_3SbO_7:Eu^{3+} show some shift to low diffraction degree with the increase of Eu^{3+} doping from 10 to 80 mol %. This indicates that the lattice experiences an expansion because of the substitution of the bigger Eu^{3+} (1.01 Å, CN=7) for Y^{3+} ions (0.96 Å, CN=7), which randomly distribute on the seven coordinated cation sites in Y_3SbO_7.

Figure 2 (a) is the XRD patterns of $La_{3-3x}Eu_{3x}SbO_7$ (x=0.05-0.8) phosphors. The XRD peak positions and relative intensity of the samples doped by Eu^{3+} below x=0.6 are in agreement with PDF#2 standard card number 23-1139 (La_3SbO_7) except for the shift of the pattern to high diffraction degree. However, as the doping level exceeds x=0.7, the patterns do not match the referred pattern of La_3SbO_7, which can be indexed to another substructure of PDF#2 card No.24-0420 (Gd_3SbO_7).

Figure 2 (b) illustrates the variation of the unit cell lattice parameter a on the Eu^{3+} doping concentrations in $La_{3-3x}Eu_{3x}SbO_7$ (x=0.05-1.0). It is obvious that the crystal structure parameters become smaller in the sequence of x=0.05 to 1.0. The lattice experiences a shrink because the different radii of La^{3+} (1.10 Å) and Eu^{3+} (1.01 Å) distributed on the cation sites in the lattices. This shrink can be clearly seen from the high degree-shift of the patterns as shown inset in Fig. 2 (b) in two theta 28-30^o. In the doping region of $0.05 \leq x \leq 0.6$, the XRD patterns show a clear double diffraction peaks of the (024)/(204), which is typical for the orthorhombic C*mcm* structure for La_3SbO_7. Only one XRD peak is observed in the two theta degree (28-30^o) as shown in the inset of Fig. 1 when the doping level is $x \geq 0.8$. This indicates that the crystal phase was induced to a Gd_3SbO_7 structure when Eu^{3+} doping above 80 mol% in La_3SbO_7.

It can be seen that over the composition range of $0.05 \leq x \leq 1$ the dependence of unit cell parameter a on doping level does obey Vegard's rule,[18] i.e., there is an obvious break point at x=0.7. In each region of $0.05 \leq x \leq 0.7$ and $0.7 \leq x \leq 1.0$, the substitution of Eu^{3+} in two cation sublattice obeys excellent Vegard's rule for structural parameters with the linear fitting factors R^2 0.9949 and 0.9976, respectively. This confirms the two crystal phases were separated at the doping shed at x=0.7.

The representative profiles of XRD structural refinements of $La_{2.7}Eu_{0.3}SbO_7$ and $Y_{2.7}Eu_{0.3}SbO_7$ were carried out using GSAS program.[17] The structure of R_3SbO_7 has a wide variety, which was

supposed to derive from fluorite structure $M_4^{4+}O_8$ by the substitution of R^{3+} and Sb^{5+} for M^{4+} ions.[15] It can be seen that XRD patterns of Y_3SbO_7 and Gd_3SbO_7 in Fig. 1 are in agreement with PDF#2 card No.24-0420, which was reported by D. K. Nath.[19] In this reference a cubic space group of Fd-3m was supposed to Gd_3SbO_7. However, no atomic coordinates were reported for any of the reported compounds. Rossell[20] determined the crystal structure of Y_2GdSbO_7 with the space group $C222_1$. The space group of $C222_1$ for Ho_3SbO_7 and Dy_3SbO_7 was adopted by Fennell et al[16] in their investigations of the structure and magnetic properties of the compounds. Recently, Hinatsu et al [15] reported the detailed crystal structure and magnetic properties of ternary Ln_3SbO_7 (Ln=Rare earths). Ln_3SbO_7 compounds crystallize in an orthorhombic superstructure of cubic fluorite (space group C*mcm* for Ln=La, Pr, Nd; $C222_1$ for Ln=Nd–Lu). In this work, our structural refinements were completed by the structural model with the space group C*mcm* and $C222_1$ for La_3SbO_7 and Y_3SbO_7,[15] respectively.

Figure 3 and 4 plots experimental, calculated, and difference results from the refinements of La_3SbO_7 and Y_3SbO_7, respectively. The parameters of the refinement are listed in Table 1 (La_3SbO_7) and 2 (Y_3SbO_7). The results indicate that the Eu^{3+} ions were completely incorporated into the host lattices without making significant changes to the crystal structure. The refinement parameters of the atomic coordinates and occupancies of La_3SbO_7 and Y_3SbO_7 are given in Table 3 and 4, respectively. Fig. 5 displays the structure sketch maps of Eu^{3+}-doped La_3SbO_7 and Y_3SbO_7, which was modeled using the Diamond Crystal and Molecular Structure Visualization software on the basis of the atomic coordinate's data from XRD refinements.

The compounds belong to an ordered, defect-fluorite orthorhombic superstructure. The structures have features in common for both the compounds. The SbO_6 octahedra share one oxygen ion (O(3) for La_3SbO_7 and O(5) for Y_3SbO_7), forming an infinite one-dimensional zig-zag chain parallel to the [001] direction. The La(Y)1 ions are coordinated by seven oxygen ions and the distorted La(Y)2-O8 also form a one-dimensional chain through edge-sharing. The SbO_6 and La(Y)2-O8 chains lie alternately parallel to the (100) plane, and the La(Y)1-O7 slabs consisting of these chains. The SbO_6 octahedra in the Sm_3SbO_7 structure are tilted along the [010] directions. The SbO_6 octahedron and Ln(2)O8 cube in the La_3SbO_7 are more regular than those in the Y_3SbO_7 structure.[15]

To confirm the crystalline morphology of Eu^{3+} doped polycrystals, SEM images were investigated. Fig. 6 (a) is a typical SEM micrograph of Eu^{3+}-doped Gd_3SbO_7 prepared at 1550 ^oC. The sample crystallized with the irregular particles. The morphology of the as-prepared grains presents smooth surface. This may be advantageous for the luminescence application. Fig. 6 (b) is the statistical size distribution of the particles. Among the calculated particles the maximum and minimum diameters of the particles are 19.52 μm and 3 μm, respectively. The average size of the particles estimated by the micrograph is about 9.27 μm.

3.2 Photoluminescence properties

Figure 7 is the representative photoluminescence excitation and emission spectra of La_3SbO_7:Eu^{3+} (a), Gd_3SbO_7:Eu^{3+} (b) and Y_3SbO_7:Eu^{3+} (c) measured under the same experimental condition at 300 K. The excitation spectrum by monitoring the $^5D_0$ emission of Eu^{3+} ions consists of a broad band at 200-350 nm and some sharp lines from the characteristic intra-configurational 4*f*–4*f* transitions: 395 nm ($^7F_0 \rightarrow {}^5L_6$), and 464 nm ($^7F_0 \rightarrow {}^5D_2$). The broad absorption band is known as

the Eu^{3+}–O^{2-} charge transfer band (CTB). Since Eu^{3+} has a $4f^6$ configuration, it needs to gain one more electron to achieve the half-filled $4f^7$ configuration, which is relatively stable compared to partially filled configurations. When Eu^{3+} is linked to the O^{2-} ligand, there is a chance of electron transfer from O^{2-} to Eu^{3+} to form Eu^{2+}–O^-. The dominated sharp excitation lines in the longer wavelength region (350–550 nm) in Fig. 7 are from the *f–f* transitions within $4f^6$ configuration of Eu^{3+} ions. Although three samples have similar excitation, obviously, the difference is the relative intensity between the intensity of CT band and *f-f* transitions. $La_3SbO_7:Eu^{3+}$ (a) phosphor has an efficient excitation intensity in the region of UV and near-UV wavelengths (*f→f* transitions of Eu^{3+}, e.g., $^7F_0 \rightarrow {}^5L_6$), which is very stronger than the absorption in the CT region. This wavelength region of 4*f*-4*f* transitions of Eu^{3+} ions can overlap with near violet (InGaN) or blue LED chip radiation. This indicates that the phosphor can well match with the excitation from UV-LED chips (360–400 nm) based on GaN semiconductor, which is essential for improving the efficiency of W-LEDs. However, in $Gd_3SbO_7:Eu^{3+}$ (b) and $Y_3SbO_7:Eu^{3+}$ (c) the CT band is stronger than *f-f* transitions. This indicates that the two phosphors have efficient excitation under UV light.

Although the three samples show the same emission transitions from the excited states $^5D_0$ to the ground states ^7F_J (J = 0, 1, 2, 3, 4) in $4f^6$ configurations of the Eu^{3+} ions, the relative intensity between each group of the transitions in each sample is very different. There are two interesting characteristics as the follows:

Firstly, $^5D_0 \rightarrow {}^7F_4$ emission peaks is the dominated transition in Eu^{3+}-doped La_3SbO_7 as shown in Fig. 7 (a). This is very different from Eu^{3+}-doped Gd_3SbO_7 and Y_3SbO_7, where the strongest emission peaks are $^5D_0 \rightarrow {}^7F_1$ (Fig. 7 b) and $^5D_0 \rightarrow {}^7F_0$ (Fig. 7 c), respectively. The dominated transitions from $^5D_0 \rightarrow {}^7F_4$ are not so often in emission spectra of Eu^{3+} ions. In Eu^{3+}-doped $Na_9[EuW_{10}O_{36}]$,[21] Eu^{3+}-doped $LaBWO_6$ [22] and $(Y_3Al_{4-x}Ga_{1-x}O_{12})$[23] the strongest $^5D_0 \rightarrow {}^7F_4$ transition of Eu^{3+} ions were observed. It was suggested to a highly polarizable chemical environment corresponding to a coordination polyhedron of Eu^{3+} ions in $LaBWO_6$ [22]. In Eu^{3+}-doped garnet $(Y_3Al_{4-x}Ga_{1-x}O_{12})$, Skaudzius et al[23] discussed the dominated $^5D_0 \rightarrow {}^7F_4$ transitions with regard to the influence of site symmetry, electronegativity (EN) and ionic radius of M^{3+} cations (M=Al, Ga and Y) in the host. The fraction of $^5D_0 \rightarrow {}^7F_4$ transition with respect to the whole emission spectrum increases with increasing average EN values of M^{3+} ions.[21] In present work, this abnormal intensity from $^5D_0 \rightarrow {}^7F_4$ has not a clear explanation; however, it is reasonable that the environment around Eu^{3+} ions could be influenced by the nature lattice of host in La_3SbO_7.

Secondly, $^5D_0 \rightarrow {}^7F_0$ of Eu^{3+} ions transition in Y-compounds is usually strong. It has been well confirmed that $^5D_0 \rightarrow {}^7F_0$ is highly forbidden for both electric-dipole (ED) and magnetic-dipole (MD) transition in a Eu^{3+}-doped compound.[24-26] However, $^5D_0 \rightarrow {}^7F_0$ in Eu^{3+}-doped Y_3SbO_7 presents the strongest transition intensity at 580 nm (Fig. 7 c). Based on Judd-Ofelt theory,[25,26] $^5D_0 \rightarrow {}^7F_0$ in Eu^{3+}-doped compounds is highly forbidden for both electric-dipole (ED) and magnetic-dipole (MD) transition.[27,28] This abnormal phenomenon has a big departure from Judd-Ofelt theory. The unusually strongest $^5D_0 \rightarrow {}^7F_0$ transitions have been reported in other materials,[29-31] for example, Eu^{3+}-doped Ba_2SiO_4,[32] $La_2Si_2O_7$,[33] $BiCa_4(PO_4)_3O$,[34] $CuLaO_2$,[35] BaFCl microcrystals[27]. There are different explanations for this origin. Firstly, this phenomenon has been ascribed to several competing mechanisms involving the mixing of two different states with different J values (J mixing), the breakdown of the closure approximation and/or Wybourne-Downer mechanism and relativistic effects.[35-37] Secondly, a series of observations of strong $^5D_0 \rightarrow {}^7F_0$ lines of Eu^{3+} ions occupying some particular symmetry sites (C_s, C_n, C_{nv}, n=1, 2,

3, 4, and 6) of crystalline or glass which allows a linear CF parameter have been reported.[38] Thirdly, the microstructure can also induce this strong transition, for example, the abnormal strong intensity of $^5D_0 \rightarrow {}^7F_0$ transition in $BiCa_4(PO_4)_3O$ apatite was ascribed to the high covalent Eu^{3+}–O^{2-} bond that is formed.[34] In Y_3SbO_7, Eu^{3+} ions were doped in distorted Y-O polyhedral. It is reasonable that the Y_3SbO_7 lattices have enough space to accommodate extra oxygen because the sample was prepared in air atmosphere. The extra oxygen in the lattices could be responsible for the unusually strongest $^5D_0 \rightarrow {}^7F_0$ transitions in Eu^{3+}-doped Y_3SbO_7.

3.3 High concentration quenching

The integrated intensity for each emission spectrum (I_{em}) was labeled in Fig. 7. It can be seen that under the same conditions luminescence of Eu^{3+}-doped La_3SbO_7 presents much higher intensity than the other two phosphors. Eu^{3+}-doped Y_3SbO_7 has the lowest luminescence intensity. The integral emission intensity of La_3SbO_7:Eu^{3+} is nearly 5.5 and 7.2 times higher than that of Gd_3SbO_7:Eu^{3+} and Y_3SbO_7:Eu^{3+} as shown in Fig. 7.

Figure 8 shows the detailed PL QEs of R_3SbO_7:$x$$Eu^{3+}$ (R= La, Gd, Y) as a function of Eu^{3+} doping concentration (x=0.05-1.0). The luminescence efficiency increases with the increase of Eu^{3+} doping and the summit appears at about x=0.4. However, the luminescence intensity decreases when x>0.4. This is due to the well-known concentration quenching in RE ions doped phosphors.

It can be noted that the La_3SbO_7:0.4Eu^{3+} shows the absolutely higher QE than Eu^{3+}-doped Gd_3SbO_7 and Y_3SbO_7 phosphors. The maximum PL QE value (excitation at 254 nm) was measured to be 63.8 % in La_3SbO_7:0.4Eu^{3+} at room temperature. However, QEs of Gd_3SbO_7:0.4Eu^{3+} of and Y_3SbO_7:0.4Eu^{3+} are 17.1 % and 10.9%, respectively. When the Eu^{3+} doping concentration is higher above 40 mol %, the luminescence intensity only decreases a little in R_3SbO_7:$x$$Eu^{3+}$ (R= Gd, Y). However, the luminescence of La_3SbO_7:$x$$Eu^{3+}$ shows an abrupt decrease at Eu^{3+} doping x=0.7. This is due to that the new crystal phase was created from C*mcm* to $C222_1$ as shown in XRD results in Fig. 2. It is well-known that the host crystal structure has a vital influence on the efficiency in RE ions activated phosphors; the other factors such as preparation conditions etc only exert small influences to some extent. In our experiments, the samples were prepared under the same conditions, consequently it can be concluded that Eu^{3+} ions as activators have very high luminescence efficiency in C*mcm* phase than those in $C222_1$ phase. The detailed differences will be introduced in the following discussion section.

The optimum Eu^{3+} doping level is decided to be 40 mol %. The high doping of Eu^{3+} ions in a phosphor can suffer high power excitation in the applications in W-LEDs, especially large power ones. The quenching concentration of Eu^{3+} doping in RPO_4:Eu^{3+} (R=La, Gd, Y) and Y_2O_2S:Eu^{3+} is only 5.0 mol %.[39] According to Dexter[40] the decay of the luminescence intensity is a result induced by the non-radiative energy transfer between the two adjacent sensitizers. Thus, the critical distance (R_c) could be calculated by the equation as following:

$$R_c \approx 2\left[\frac{3V}{4\pi X_C Z}\right]^{\frac{1}{3}} \qquad (1)$$

where V is the volume of the unit cell, X_c is the critical concentration of the activator ion, Z is the number of formula unit per unit cell. For R_3SbO_7:$x$$Eu^{3+}$ (R= La, Gd, Y) host, the values of Z and χ_c are 4 and 0.4, respectively. The critical transfer distances of Eu^{3+} luminescence quenching in R_3SbO_7:$x$$Eu^{3+}$ hosts are 9.18 Å (R=La), 9.03 Å (R=Gd), 8.85 Å (R=Y).

Non-radiative energy transfer often occurs by an exchange interaction, a radiation re-absorption, or a multipole-multipole interaction. The exchange interaction is generally responsible for the energy transfer of forbidden transitions and the typical critical distance is about 5 Å.[40] The calculated average distance between the Eu^{3+} ions are all larger than 5 Å, which means the exchange interaction becomes ineffective. And it also hampers the excitation energy migration making the high concentration quenching possible in the R_3SbO_7:xEu^{3+} (R= La, Gd, Y).

Usually the concentration quenching is strongly dependent on the structural dimensionality of the host. There is a weak concentration quenching of europium luminescence in the host, where the RE ions could form a quasi-two-dimensional $RE(Eu)^{3+}$ sublattice.[41] In the structure of R_3SbO_7:xEu^{3+} (R= La, Gd, Y), the cation sites R1 and R2 form the layer structure in the perpendicular [001] direction. The energy transfer might be restricted to the quasi-two-dimensional Eu^{3+} sublattice in this host.

The thermal stability of a phosphor is one of the important factors because it could be used in a higher working temperature, e.g., 100-150 °C. The high temperature could result in thermal quenching by nonradiative transition from the excited to the ground states of Eu^{3+} ions.[42,43] Fig. 9 is the normalized integrated emission intensities on the temperatures. The luminescence intensities of three phosphors at 150 °C decrease to 75-80 % of the initial value (20 °C). The phosphors show a good thermal stability on the temperature quenching.

3.4 Spectrum evolution of R_3SbO_7:Eu^{3+} on doping concentration

As shown in Fig. 1 and 2, the crystal phases of La_3SbO_7:xEu^{3+} have a graduate changes on the increase of Eu^{3+}-doping. This should have a reflectance on the emission spectra of Eu^{3+} ions. Fig. 10 shows the spectra evolution of R_3SbO_7:xEu^{3+}, (R=La, Gd, and Y) as a function of Eu^{3+} doping concentration (x=0.05-1.0).

In Eu^{3+}-doped La_3SbO_7 (Fig. 10 a), the dominated emission transition of $^5D_0 \rightarrow {}^7F_4$ at 710 nm becomes weaker as the increase of Eu^{3+} doping, which is lower than that of $^5D_0 \rightarrow {}^7F_2$ as x is above 0.7. This indicates that the dominated emission transition of $^5D_0 \rightarrow {}^7F_4$ only can be observed in the *Cmcm* orthorhombic crystal phase of La-compound. Meanwhile, the relative intensity of $^5D_0 \rightarrow {}^7F_1$ emission transitions increase with the increase of the Eu^{3+}-doping, indicating the symmetry of the crystal environment of Eu^{3+} ions become higher. Fig. 10 (b) is the emission spectra of Eu^{3+}-doped Gd_3SbO_7 with different Eu^{3+} doping. All the luminescence spectra are similar to those of (70-100 mol %) Eu^{3+}-doped La_3SbO_7. The maximum emission peak is for the magnetic dipole transition $^5D_0 \rightarrow {}^7F_1$, which is not much affected by the ligand field around Eu^{3+} because of very close radii of two RE ions. In the spectra of Eu^{3+}-doped Y_3SbO_7 (Fig. 10 c), $^5D_0 \rightarrow {}^7F_0$ presents the usually strongest intensity when the Eu^{3+} doping x from 0.05 to 0.6. It turns to the similar spectra to that of Eu^{3+}-doped Gd_3SbO_7 with $x > 0.7$.

The changes of emission spectra on Eu^{3+} doping bring out the rich luminescence colors for the Eu^{3+}-doped R_3SbO_7:xEu^{3+}, (R=La, Gd, and Y) phosphors. Based on the emission spectra of La_3SbO_7:xEu^{3+} (x=0.05-1) phosphors in Fig. 10 under the excitation at 254 nm in Commission Internationale de l'Ecairage (CIE) coordinates were well calculated. Fig. 11 displays the CIE color coordinates of R_3SbO_7:xEu^{3+} (R=La, Gd, and Y). It can be observed that the amount of Eu^{3+} ions has an influence on the position of color point in this diagram. The CIE of Eu^{3+}-doped Gd_3SbO_7 phosphors keep a stable value of about (x=0.647, y=0.372), which are close to the standard of NTSC (x=0.67, y=0.33). However, Eu^{3+}-doped La_3SbO_7 and Y_3SbO_7 have tunable emission colors

as changing Eu^{3+} doping levels as shown in Fig. 11. Especially $Y_3SbO_7:Eu^{3+}$ changes its emission color from reddish-orange to deep red with increasing the doping levels of Eu^{3+} from 0.05 to 1.0.

3.5 Decay curves and Lifetimes

The fluorescence decay curves of the $^5D_0$ states in $R_3SbO_7:xEu^{3+}$ (R=La, Gd, and Y) were measured under the excitation of 266 nm Nd:YAG pulsed laser at 300 K. Fig. 12 shows the selected luminescence decay curves of $^5D_0$ states as a function of Eu^{3+} doping concentration. Three samples have similar decay curves profiles. When the Eu^{3+} concentration is low ($x < 0.3$), the decay curves are single-exponential, the curves show an exponential characteristics. This can be fitted by a single-exponential function as

$$I = I_0 \exp[-t/\tau] \quad (2)$$

I_0 is the initial emission intensity for $t = 0$. The lifetimes of Eu^{3+} in R_3SbO_7 were calculated to be 2.33, 3.26 and 3.51 ms for R= La, Gd, and Y, respectively.

With the increase of Eu^{3+} doping, the luminescence decay curves from $^5D_0$ present a non-exponential profile as shown in Fig. 12. This suggests the presence of thermally activated energy transfer process. The decay value can be given to the average lifetime defined as:

$$\tau_{avg} = \frac{\int_0^\infty tI(t)dt}{\int_0^\infty I(t)dt} \quad (3)$$

All the luminescence decay lifetimes of Eu^{3+} ($^5D_0$) werecalculated and shown in Fig. 13, which were short enough as Eu^{3+}-doped red phosphors for potential applications in displays and lightings.

4. Discussions

As shown the results above, three phosphors have distinct luminescence characteristics; Eu^{3+} could obtain highly efficient luminescence in R_3SbO_7 Cmcm phase (R=La) than that in $C222_1$ phase (R=Gd, Y). The luminescence spectra in the hosts have great and interesting differences. It is well known that the selection rules and *f-f* transition probabilities between states depend strongly on the crystal field around Eu^{3+} ions.[44] Consequently the difference of the Eu^{3+} luminescence is due to the different microstructure around Eu^{3+} ions. The attention should be paid on the R sites in the lattices because they have the similar orthorhombic defect-fluorite superstructure. R_3SbO_7 (R=La, Gd, Y) show a variety of crystal structures due to the ordering between R and Sb cations with significantly different R sizes and the formation of cation ordering occurs on the metal sites and the oxide-vacancy orders on the anion sites.[15]

For large rare-earth La_3SbO_7 has a Cmcm unit cell where La and Sb cations are distributed in order in the framework. A decrease of the ionic radius of R=Gd, Y cations leads to an orthorhombic $C222_1$ structure, which contains a framework of corner sharing $(Gd,Y)1O_7$ and $(Gd,Y)2O_8$. There is an interesting result, which has been confirmed by Yukio Hinatsu et al[15], i.e., the average Sb-O bond length in R_3SbO_7 is a constant (2.00 Å) from R=La^{3+} to Lu^{3+} in both C*mcm* and $C222_1$ phases. In this case, the obvious luminescence changes of Eu^{3+} ions in R_3SbO_7 should be related to the average distance between R(Eu^{3+}) cations and oxygen. As seen in Fig. 5, the

average distance of La-O in Cmcm phase (La1-O=2.4541 Å; La2-O=2.8182 Å) is longer than Y-O (Y1-O=2.2927 Å; Y2-O=2.4573 Å). It is well known that CT energy decreases with large average distance to the surrounding anions.[45] This is also can be reflected by the CT band shift for $R_3SbO_7:Eu^{3+}$ (*R*=La, Gd, Y) in Fig. 7. The observed CT band shifting to lower energy from $Y_3SbO_7:Eu^{3+}$ to $Gd_3SbO_7:Eu^{3+}$ and $La_3SbO_7:Eu^{3+}$ attributed to the longer Eu–O bond length.

In $Y_3SbO_7:Eu^{3+}$ the decrease of Eu-O distance could induce the highly polarizable chemical environment when Eu^{3+} was doped in Y sites. Meanwhile the space of the oxide-vacancy ordered on the anion sites in $Y_3SbO_7:Eu^{3+}$ lattices could become big enough to for the accommodation of interstitial oxygen.[21] Consequently, the high covalent Eu^{3+}–O^{2-} bond and the free O^{2-} in the lattices are responsible for the abnormal strong intensity of $^5D_0 \rightarrow {}^7F_0$ transition in $Y_3SbO_7:Eu^{3+}$.

The electric cloud of Eu^{3+} ion doesn't have the spherical symmetry originated from the incomplete 4*f* shell, which is different from La^{3+} with a spherical electron distribution. Therefore, the environment around Eu^{3+} could tend to be distorted toward a lower symmetry. In La_3SbO_7 (*R*=, Gd, Y) La cations have a formation of cation ordering. La2 site (Wyckoff Symbol 4a) has a regular polyhedral in Cmcm structure La_3SbO_7, however, the surroundingcan be distorted by the oxide-vacancy orders on the anion sites in such an orthorhombic defect-fluorite superstructure.[15] The Eu^{3+} ion in La_3SbO_7 (*R*=, Gd, Y) was doped in a cation with a center of inversion and kept distorting the chemical environment toward a lower symmetry. Consequently the dominated $^5D_0 \rightarrow {}^7F_4$ transitions of Eu^{3+} ions in La_3SbO_7 can be observed by referring the similar mechanism in $Na_9[EuW_{10}O_{36}]$.[21]

The average lifetimes of Eu^{3+} emission from the $^5D_0$ states in $R_3SbO_7:xEu^{3+}$ (*R*=La, Gd, Y) always decrease as the growing of Eu^{3+} addition. However, it can be divided into three step regions. The first is at the initial stage from *x*=0.05 to 0.2: the luminescence decay curves show the exponential characteristics with the similar lifetime values. As the doping of Eu^{3+} increase to *x*=0.3, the lifetime shows a decrease. Then the decay keeps the comparable luminescence lifetime value from *x*=0.3 to 0.6. Then a quenching can be observed as the sharp drop of lifetime when the doping is increased to *x*=0.7.

As calculated in Eq. (2), the critical transfer distances of Eu^{3+} luminescence quenching in $R_3SbO_7:xEu^{3+}$ hosts are 9.18 Å (*A*=La), 9.03 Å (*A*=Gd), 8.85 Å (*A*=Y). This indicates there is enough space for Eu^{3+} to form isolated luminescence center in the R_3SbO_7 host lattices when the doping *x* is below 0.3. For example, the maximum distance between two close neighbors in the La_3SbO_7 lattices is 6.7359 Å. Consequently we can assign the Eu^{3+} ions are doped as isolated luminescence centers when the doping is below 0.3. Eu^{3+} emission lifetimes from the $^5D_0$ states in $R_3SbO_7:xEu^{3+}$ (*x*=0.3-0.6) become shorter with non-exponential properties. This is induced by the pair broadening effects in the lattices because of Eu^{3+} ions get closer and closer. The luminescence centers of Eu^{3+} cannot be avoidable because of the special spatial arrangement for the corner-shared $R1O_7$ and $R2O_8$ polyhedral.

For high Eu^{3+}-concentration (*x* >0.7) phosphors, the non-exponential decay curves and similar lifetime values of the sample with *x*=0.7-1.0 imply that the energy migration takes place in host lattices.[46] In this case Eu^{3+} luminescence cluster centers can be formed in the R_3SbO_7 lattices. This bring out the completely luminescence quenching in $R_3SbO_7:xEu^{3+}$ (*R*=La, Gd, and Y). There are multi-sites for Eu^{3+} ions in R_3SbO_7 because there are two kinds of *R* sites available in host lattice. To elucidate the detailed luminescence mechanism, the detailed site-assignment and luminescence contributions can be investigated in the future by the site-selective excitation and emission

technique by pulsed dye laser in the $^5D_0 \rightarrow {}^7F_0$ transition region.

5. Conclusions

Polycrystalline rare earth antimonates $R_{3-3x}Eu_{3x}SbO_7$ (R=La, Gd, Y, x=0.05-1.0) were synthesized via the solid-state reaction. The emission spectrum of Eu^{3+}-doped La_3SbO_7 is dominated by $^5D_0 \rightarrow {}^7F_4$ transition (710 nm); In Eu^{3+}-doped Gd_3SbO_7, the maximum emission peak is for the magnetic dipole transition $^5D_0 \rightarrow {}^7F_1$. However, $^5D_0 \rightarrow {}^7F_0$ presents the usually strongest intensity in the spectrum of Eu^{3+}-doped Y_3SbO_7. R_3SbO_7:$x$$Eu^{3+}$ (R= La, Gd, Y) has an optimum Eu^{3+} doping level of 40 mol %. The Eu^{3+} ions doped in C*mcm* phase have much higher luminescence efficiencies than those doped in $C222_1$ phase. The maximum photoluminescence QE value was measured to be 63.8 % in La_3SbO_7:$0.4Eu^{3+}$ at room temperature. La_3SbO_7:xEu^{3+} has a tunable luminescence color dependent on the Eu^{3+} doping levels. The spectral characteristic was discussed on the base of the crystal structure and micro-surrounding of Eu^{3+} ions. Eu^{3+} ions present isolated color center in lowing doping, and induce a pair broadening effect with increasing the doping; In Eu^{3+}-heavily doped sample, cluster centers can be formed inducing luminescence quenching.

Acknowledgments

This work was supported by Basic Science Research Program through the National Research Foundation of Korea (NRF) funded by the Ministry of Science, ICT & Future Planning (NRF-2013R1A1A2009154) and by the Priority Academic Program Development of Jiangsu Higher Education Institutions (PAPD), China. We give thanks to Dr. Liang Shi in Saint-Gobain Research (Shanghai, China) Co. Ltd. for the help of some luminescence measurements.

References

1 S. P. Wen, X. P. Zhang, L. Yao, M. Xi, L. Q. Zhang, H. Fong and L. Liu, *J. Mater. Chem. C*, 2013, 1, 1613.

2 Y. Zhou, B. Yan and X. H. He, *J. Mater. Chem. C*, 2014, 2, 848.

3 L. N. Guo, Y. H. Wang, L. L Han, Q. P. Qiang, W. Zeng, Z. H. Zou, B. Wang and X. X. Guo, *J. Mater. Chem. C*, 2013, 1, 7952.

4 D. Geng, M. M. Shang, Y. Zhang, H. Z. Lian, Z. Y. Cheng and J. Lin, *J. Mater. Chem. C*, 2013, 1, 2345.

5 J. C. Zhang, Y. Z. Long, H. D. Zhang, B. Sun, W. P. Han and X. Y. Sun, *J. Mater. Chem. C*, 2014, 2, 312.

6 T. Justel, H. Nikol and C. Ronda, *Angew. Chem. Int. Ed*, 1998, 37, 3084.

7 C. Ronda, in *Wiley-VCH: Weinheim, Germany*, ed. C. Ronda, 2008.

8 S. K. Mahesh, P. P. Rao, M. Thomas, T. L. Francis and P. Koshy, *Inorg. Chem*., 2013, 52, 13304.
9 H. Y. Lin, Y. C. Fang, X. R. Huang and S. Y. Chu, *J. Am. Ceram. Soc.*, 2010, 93, 138.
10 F. Du, R .Zhu, Y. L. Huang, Y. Tao and H. J. Seo, *Dalton Trans*., 2011, 40, 11433.
11 X. Y. Chen and G. K. Liu, *J. Solid State Chem.*, 2005, 178, 419.
12 M. Hirayama, N. Sonoyama, A. Yamada and R. Kanno, *J. Lumin*., 2008, 128, 1819.
13 A. M. Srivastava, *Opt. Mater*., 2009, 31, 881.
14 A. Kahn-Harari, L. Mazerrolles, D. Michel and F. Robert, *J. Solid State Chem.*, 1995, 116, 103.
15 Y. Hinatsu, H. Ebisawa and Y. Doi, *J. Solid State Chem.*, 2009, 182, 1694.
16 T. Fennell, S. T. Bramwell and M. A. Green, *Can. J. Phys*., 2001, 79, 1415.
17 A. C. Larson and R. B. Von Dreele, in *LAUR*, 1994, pp. 86-748.
18 R. E., Smallman, in *Modern Physical Metallurgy*, 4th edn., 1985.
19 D. K. Nath, Inorg. Chem., 1970, 9(12), 2714-2718
20 H.J. Rossell, J. Solid State Chem., 1979, 27, 115–122.
21 R. A. SaFerreira, S. S. Nobre, C. M. Granadeiro, H. I. S. Nogueira, L. D. Carlos and O. L. Malta, *J. Lumin.*, 2006, 121, 561.
22 Y. Huang, H. J. Seo, Mater. Lett., 2012, 84, 107.
23 R. Skaudzius, A. Katelnikovas, D. Enseling, A. Kareiva and T. Jüstel, *J. Lumin*., 2014, 147, 290.
24 B. G. Wybourne, *J. Alloys Compd*., 2004, 380, 96.
25 G. S. Ofelt, *J. Chem.Phys*., 1962, 37, 511.
26 B. R. Judd, *Phys. Rev*., 1962, 127, 750.
27 X. Y. Chen, W. Zhao, R. E. Cook and G. K. Liu, *Phy. Rev. B*, 2004, 70, 205122.
28 P. A. Tanner, Y. Y. Yeung and L. Ning, *J. Phys. Chem. A*, 2013, 117, 2771.
29 L. Smentek and A. Kędziorski, *J. Alloys Compd*., 2009, 488, 586.
30 A. S. Souza, Y. A. R. Oliveira and M. A. Couto dos Santos, *Opt. Mater.*, 2013, 35, 1633.
31 A. K. Parchur and R. S. Ningthoujam, *RSC Adv*., 2012, 2, 10859.
32 A. M. Pires, M. R. Davolos and O. L. Malta, *J. Lumin*., 1997, 72-74, 244.
33 B. Piriou, M. Richard-Plouet, J. Parmentier, F. Ferey and S. Vilminot, *J. Alloys Compd*., 1997, 262-263, 450.
34 N. Lakshminarasimhan and U.V. Varadaraju, *J. Solid State Chem*., 2004, 177, 3536.
35 F. Fujishiro, R. Sekimoto and T. Hashimoto, *J Lumin*., 2013, 133, 217.
36 F. Fujishiro, M. Murakami, T. Hashimoto and M. Takahashi, *J Ceram Soc Jpn*., 2010, 118, 1217.
37 M. C Downer, G. W Burdick and D. K Sardar, *J. Chem.Phys*., 1988, 89, 1787.
38 N. J. Cockroft, S. H. Lee and J. C. Wright, *Phys. Rev. B*, 1991, 44, 4117.
39 U. Rambabu and S. Buddhudu, *Opt. Mater*., 2001, 17, 401.
40 D. L. Dexter, J. *Chem. Phys.,* 1953, 21, 836.
41 K. Toda, Y. Kameo, M. Ohta and M. Sato, *J. Alloys. Compd*., 1995, 218, 228.
42 C. C. Lin, R. S.Liu, J. Phys. Chem. Lett., 2011, 2, 1268.
43 A. A. Setlur, H. A. Comanzo, A. M. Srivastava, W. W. Beers, J. Electrochem. Soc., 2005, 152, H205.
44 C. Gorller-Walrand and K. Binnemans, *Handbook on the Physics and Chemistry of Rare Earths*, ed. K. A. Gschneidner and L. Eyring, 1996.

45 V. Jubera, J. P. Chaminade, A. Garcia, F. Guillen and C. Fouassier, *J. Lumin.*, 2003, 101, 1.
46 J. P. M. Van Vliet and G. Blasse, *J. Solid State Chem.*, 1988, 76, 160.

Table 1 Crystallographic refinement parameters of Eu^{3+}-doped La_3SbO_7.

formula	La_3SbO_7
radiation	Cu *K*a
2θ range(degree)	10-70
symmetry	orthorhombic
space group#	Cmcm (63)
a/Å	11.0895(8)
b/Å	7.5935(5)
c/Å	7.7081
α/°	90
β/°	90
γ/°	90
Z	4
R_p	0.0512
R_{wp}	0.07958
X^2	1.8917
V/ $Å^3$	649.08(8)

Table 2 Crystallographic refinement parameters of Eu^{3+}-doped Y_3SbO_7.

formula	Y_3SbO_7
radiation	Cu *K*a
2θ range(degree)	10-70
symmetry	orthorhombic
space group#	$C222_1$ (20)
a/Å	7.3958(8)
b/Å	10.442(1)
c/Å	7.4143(8)
α/°	90
β/°	90
γ/°	90
Z	4
R_p	0.0459
R_{wp}	0.0756
X^2	1.579
V/ $Å^3$	572.58(10)

Table 3 Refined atomic coordinate parameters data of Eu^{3+}-doped La_3SbO_7 at room temperature

Atom	Ox.	Wyck.	Site	x/a	y/b	z/c	U [Å^2]
O1		16h	1	0.37100	0.18000	0.03600	0.0250
O2		8g	..m	0.13900	0.02800	1/4	0.0250
La1		8g	..m	0.2300(5)	0.2938(7)	1/4	0.0122(28)
O3		4c	m2m	0	0.44900	1/4	0.0250
Sb1		4b	2/m..	0	1/2	0	0.011(5)
La2		4a	2/m..	0	0	0	0.030(5)

Table 4 Refined atomic coordinate parameters data of Eu^{3+}-doped Y_3SbO_7 at room temperature.

Atom	Ox.	Wyck.	Site	x/a	y/b	z/c	U [Å^2]
Y1		8c	1	0.23790	0.23600	0.25000	0.0191(22)
O1		8c	1	0.27300	0.39200	0.04200	0.0250
O2		8c	1	0.31500	0.35700	0.47200	0.0250
O3		4b	.2.	0	0.07700	1/4	0.0250
O4		4b	.2.	0	0.35100	1/4	0.0250
O5		4b	.2.	0	0.63000	1/4	0.0250
Sb1		4a	2..	0	0	0	0.0250
Y2		4a	2..	0.49400	0	0	0.0250

Figure captions

Fig. 1 the selected XRD patterns of Eu^{3+}-doped Y_3SbO_7 and Gd_3SbO_7. The refered standard PDF#2 card is No.24-0420 (Gd_3SbO_7).

Fig. 2 XRD patterns of the samples (a): $La_{3-3x}Eu_{3x}SbO_7$ (x=0.05-0.8). The experimental patterns were compared with the corresponding standard PDF#2 cards 23-1139; (b): Variation of unit cell parameters a of $La_{3-3x}Eu_{3x}SbO_7$ solid-solution series dependent on x values.

Fig. 3 A representative experimental (crossed) and calculated (red solid line) X-ray diffraction profiles of $La_{2.7}Eu_{0.3}SbO_7$. The difference profile is located at the bottom of the figure.

Fig. 4 A representative experimental (crossed) and calculated (red solid line) X-ray diffraction profiles of 10mol % Eu^{3+}-doped Y_3SbO_7. The difference profile is located at the bottom of the figure.

Fig 5 The sketch maps of orthorhombic Cmcm structure La_3SbO_7 (a) and orthorhombic $C222_1$ Y_3SbO_7 (b) viewed along [001]. The edge-shared cations were also displayed.

Fig. 6 (a): the typical SEM micrograph of Gd_3SbO_7:0.1Eu^{3+}. The other samples have the same particle profiles; (b): the size distribution of the sample.

Fig. 7 Photo-luminescence excitation and emission spectra of 40 mol % Eu^{3+}-doped La_3SbO_7 (a), Gd_3SbO_7 (b), and Y_3SbO_7 (c) measured under the same experimental condition at 300 K. I_{em} denotes the integrated area of the emission spectrum. The excitation is UV light 254 nm at 300 K.

Fig. 8 Luminescence quantum efficiencies of $^5D_0 \rightarrow {}^7F_J$ (J=0, 1, 2, 3, and 4) emission under the excitation of 254 nm for R_3SbO_7:Eu^{3+} (R=La, Gd, Y) as a function of Eu^{3+} doping concentration.

Fig. 9 The temperature-dependent luminescence intensities of R_3SbO_7:0.4Eu^{3+} (R=La, Gd, Y) normalized to the value at 20 °C.

Fig. 10 The spectrum evolution of R_3SbO_7:Eu^{3+}, R=La (a), Gd (b), and Y (c) as a function of Eu^{3+}

doping concentration under the excitation of 266 nm with a 570 nm filter. All the spectra were normalized to its maximum intensity and some spectra were shift upward for a clear comparison.

Fig. 11 Color CIE coordinates of R_3SbO_7:xEu^{3+} (R=La, Gd, and Y) calculated from the emission spectra in Fig. 10.

Fig. 12 Luminescence decay curves of $^5D_0$ states in R_3SbO_7:xEu^{3+}, R=La (a), Gd (b), and Y (c) as a function of Eu^{3+} doping concentration. The excitation is using 266 nm Nd:YAG pulsed laser at 300 K.

Fig. 13 Luminescence lifetime of $^5D_0$ states of Eu^{3+}-doped R_3SbO_7 (R=La, Gd, and Y) as a function of doping concentration.

Fig. 1 the selected XRD patterns of Eu^{3+}-doped Y_3SbO_7 and Gd_3SbO_7. The refered standard PDF#2 card is No.24-0420 (Gd_3SbO_7).

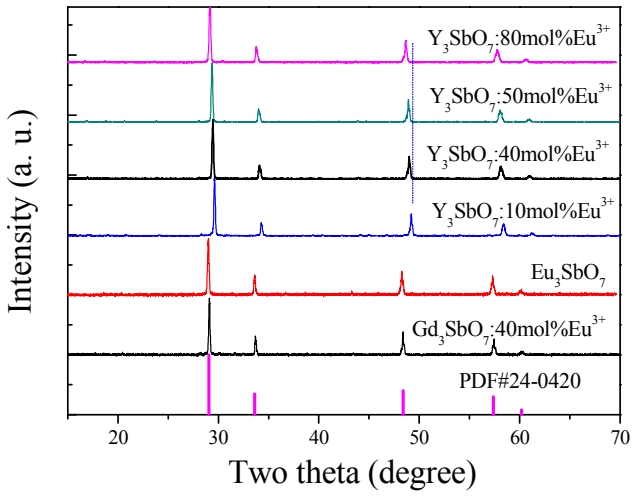

Fig. 2 XRD patterns of the samples (a): $La_{3-3x}Eu_{3x}SbO_7$ (x=0.05-0.8). The experimental patterns were compared with the corresponding standard PDF#2 cards 23-1139; (b): Variation of unit cell parameters a of $La_{3-3x}Eu_{3x}SbO_7$ solid-solution series dependent on x values.

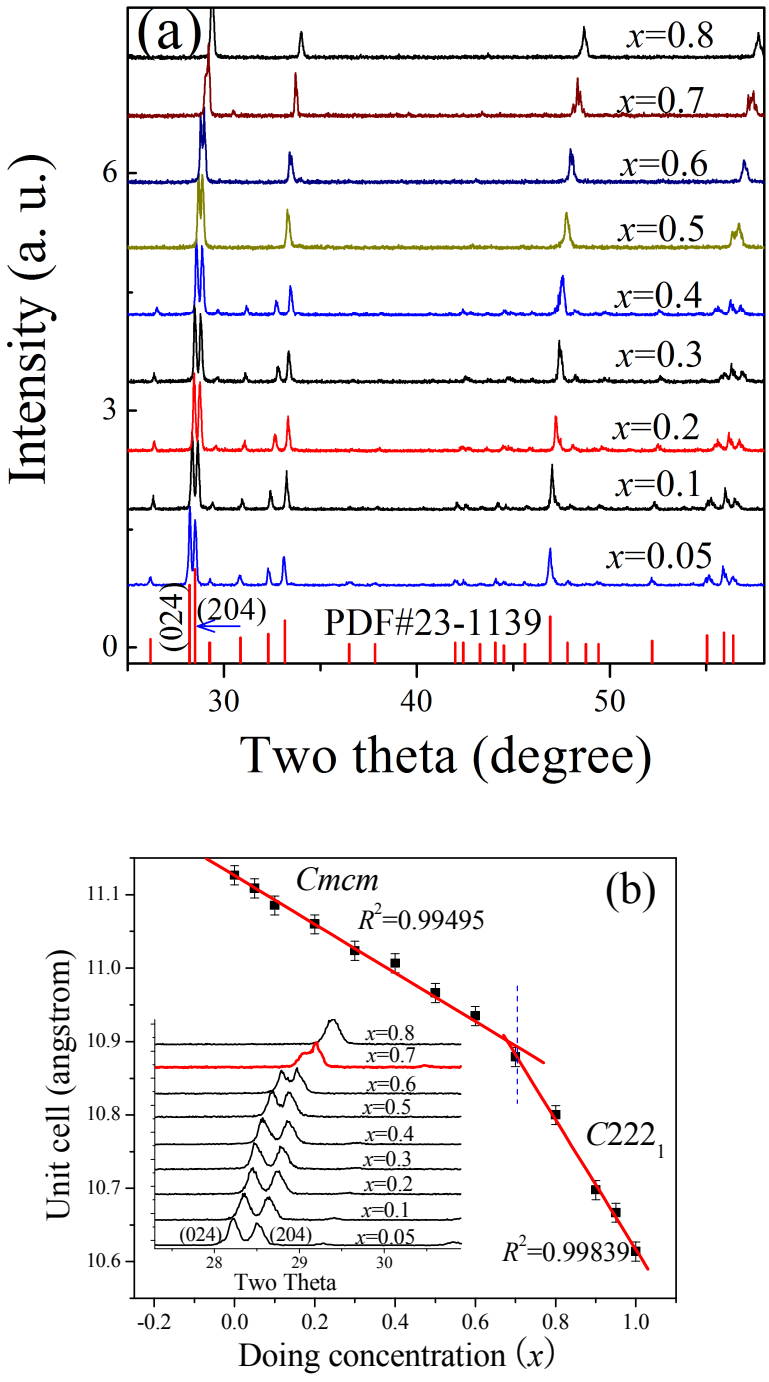

Fig. 3 A representative experimental (crossed) and calculated (red solid line) X-ray diffraction profiles of $La_{2.7}Eu_{0.3}SbO_7$. The difference profile is located at the bottom of the figure.

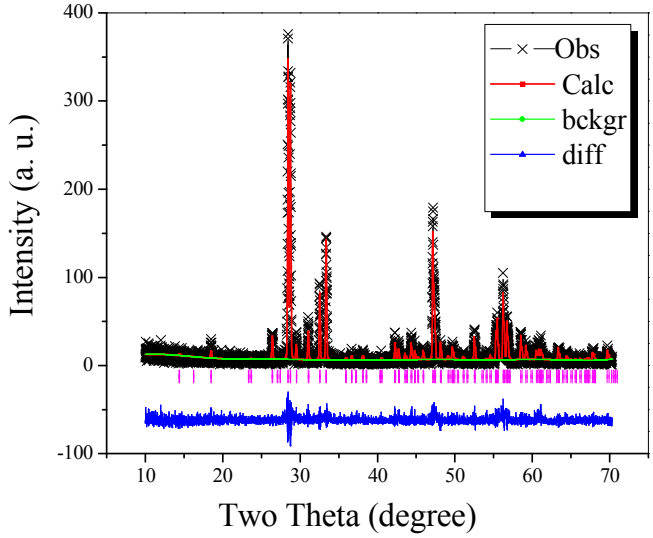

Fig. 4 A representative experimental (crossed) and calculated (red solid line) X-ray diffraction profiles of 10mol % Eu^{3+}-doped Y_3SbO_7. The difference profile is located at the bottom of the figure.

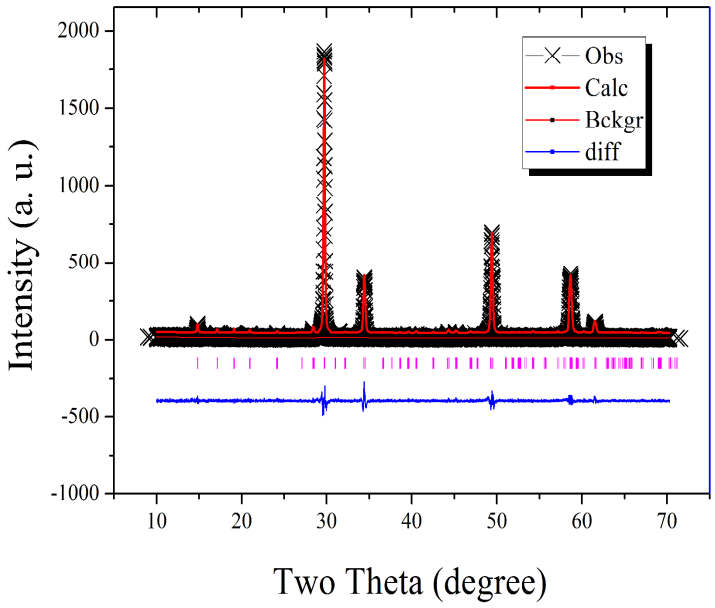

Fig 5 The sketch maps of orthorhombic Cmcm structure La_3SbO_7 (a) and orthorhombic $C222_1$ Y_3SbO_7 (b) viewed along [001]. The edge-shared cations were also displayed.

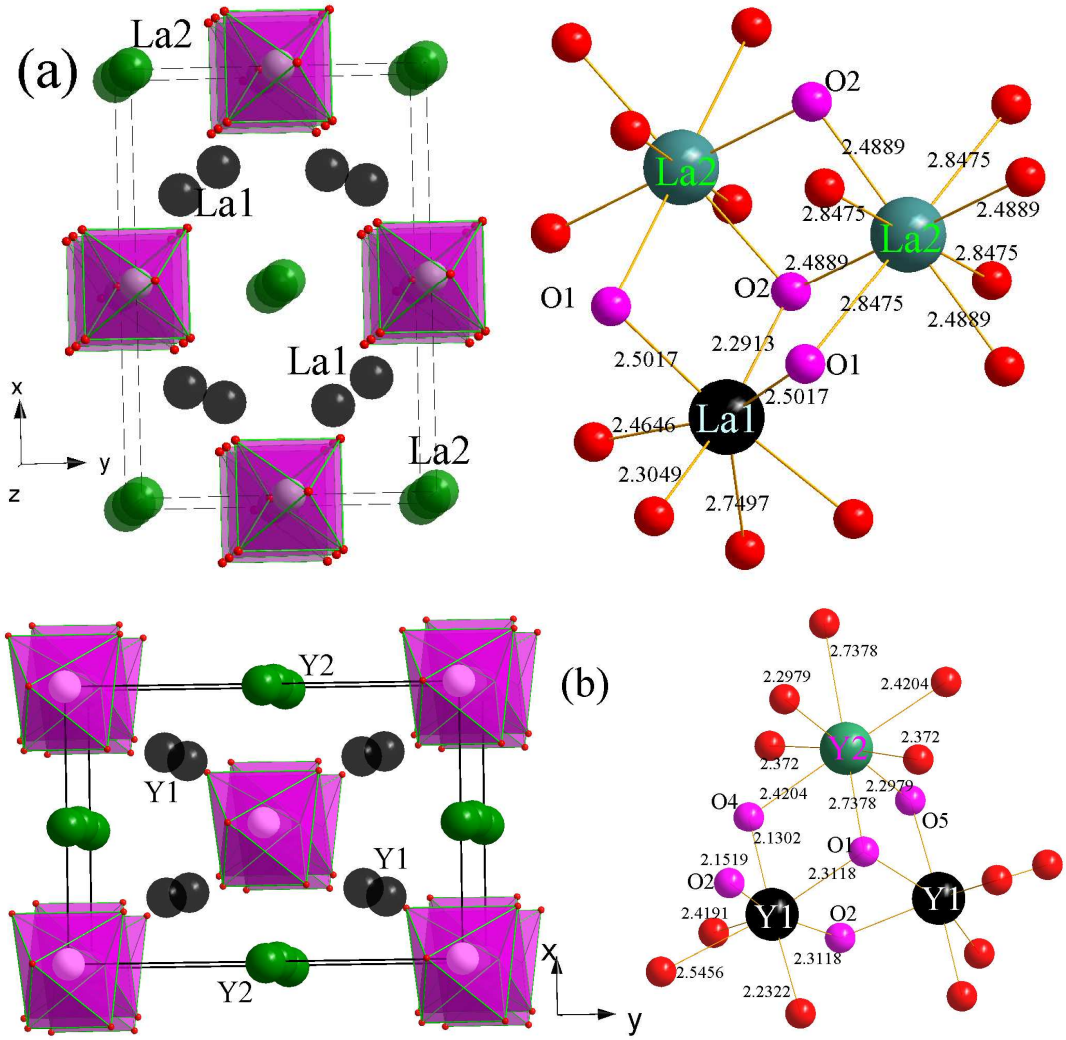

Fig. 6 (a): the typical SEM micrograph of Gd_3SbO_7:0.1Eu^{3+}. The other samples have the same particle profiles; (b): the size distribution of the sample.

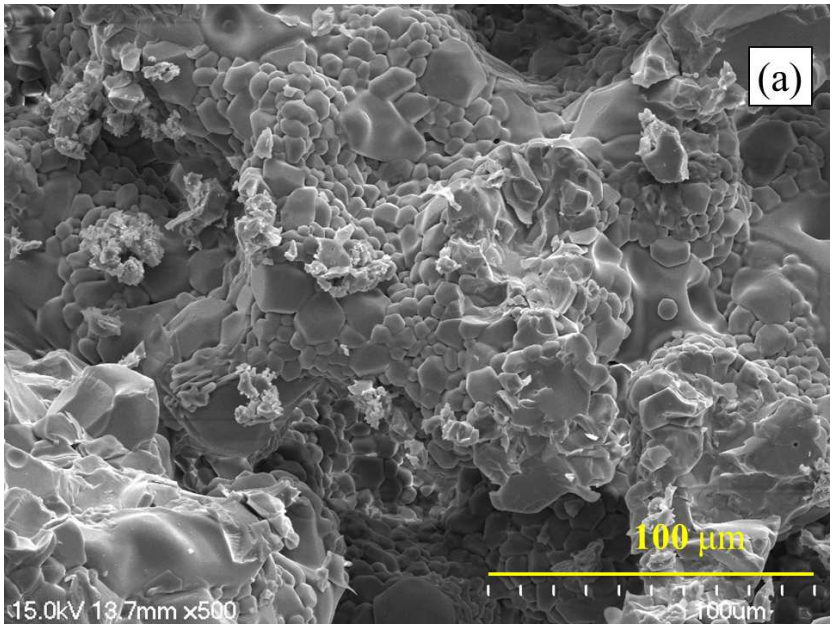

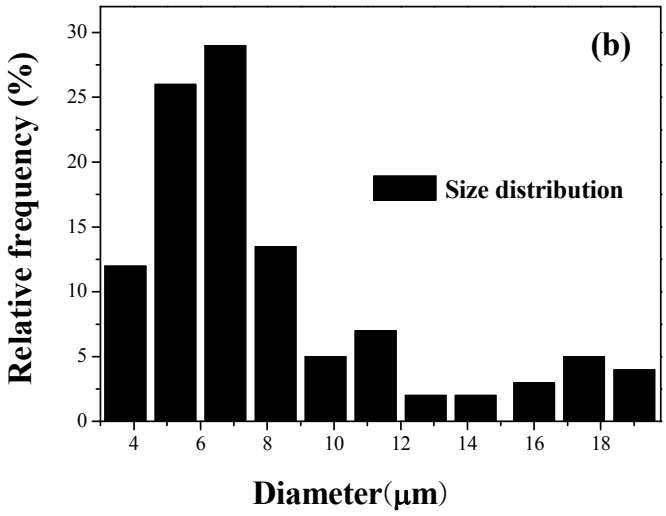

Fig. 7 Photo-luminescence excitation and emission spectra of 40 mol % Eu^{3+}-doped La_3SbO_7 (a), Gd_3SbO_7 (b), and Y_3SbO_7 (c) measured under the same experimental condition at 300 K. I_{em}

denotes the integrated area of the emission spectrum. The excitation is UV light 254 nm at 300 K.

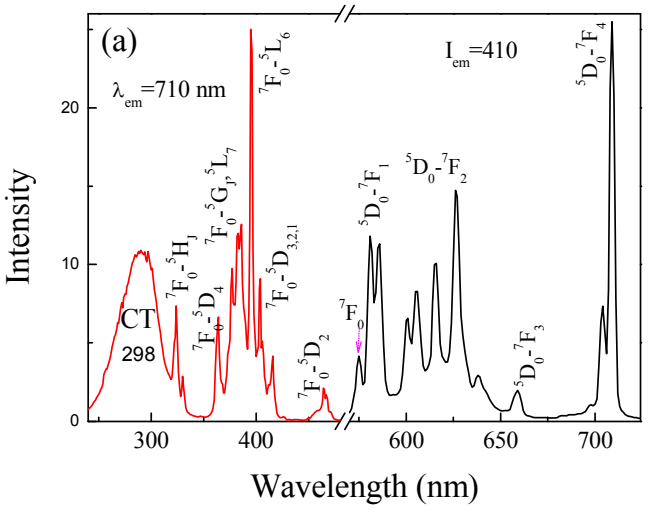

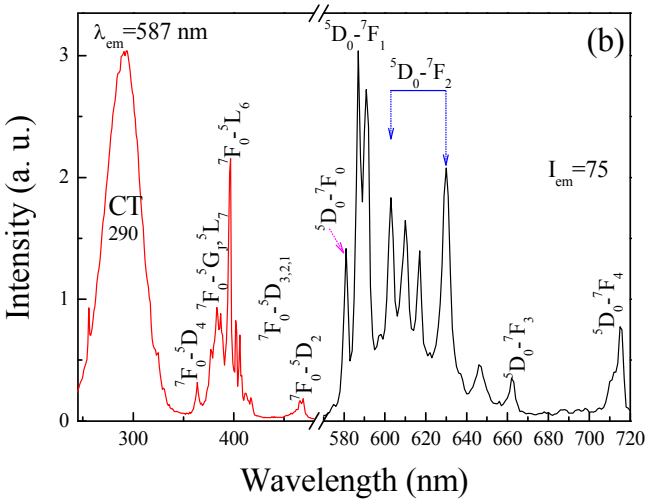

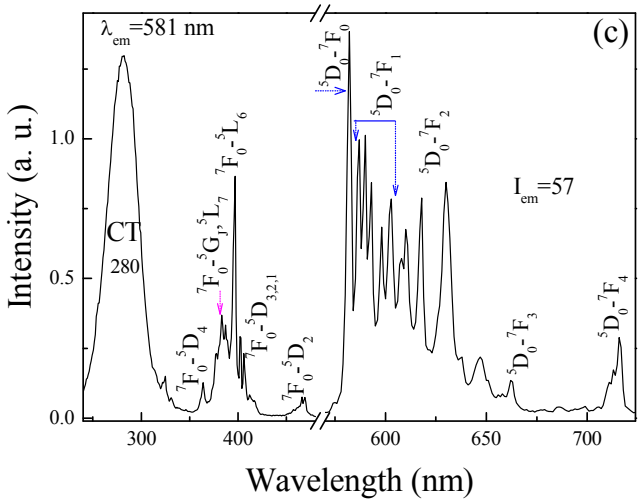

Fig. 8 Luminescence quantum efficiencies of $^5D_0 \rightarrow {}^7F_J$ (J=0, 1, 2, 3, and 4) emission under the excitation of 254 nm for $R_3SbO_7:Eu^{3+}$ (R=La, Gd, Y) as a function of Eu^{3+} doping concentration.

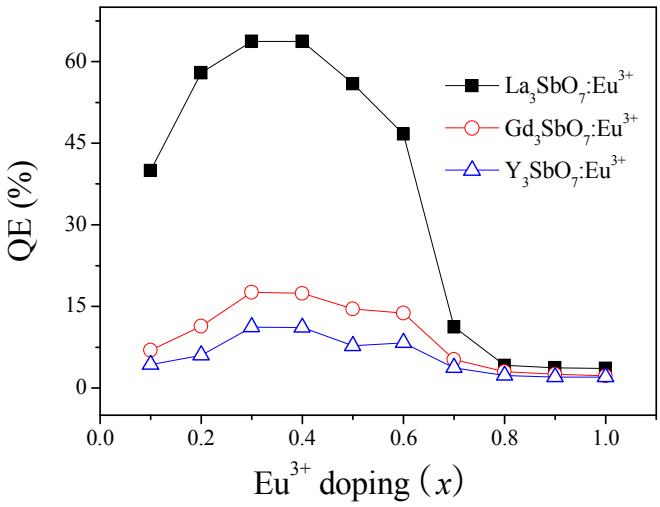

Fig. 9 The temperature-dependent luminescence intensities of R_3SbO_7:0.4Eu^{3+} (R=La, Gd, Y) normalized to the value at 20 °C.

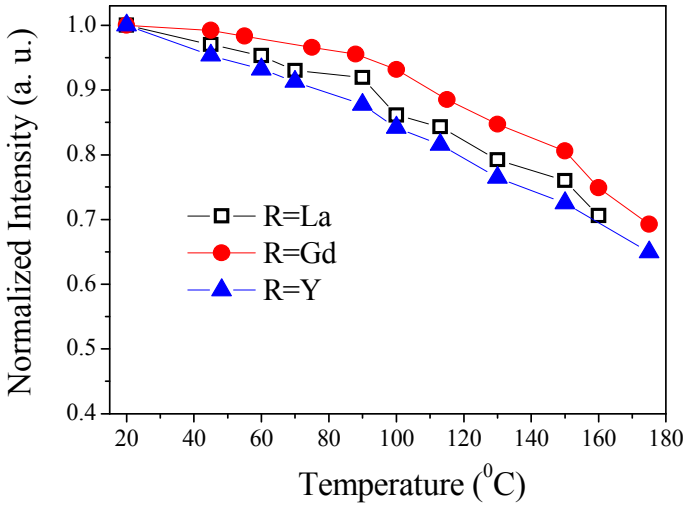

Fig. 10 The spectrum evolution of R_3SbO_7:Eu^{3+}, R=La (a), Gd (b), and Y (c) as a function of Eu^{3+} doping concentration under the excitation of 266 nm with a 570 nm filter. All the spectra were normalized to its maximum intensity and some spectra were shift upward for a clear comparison.

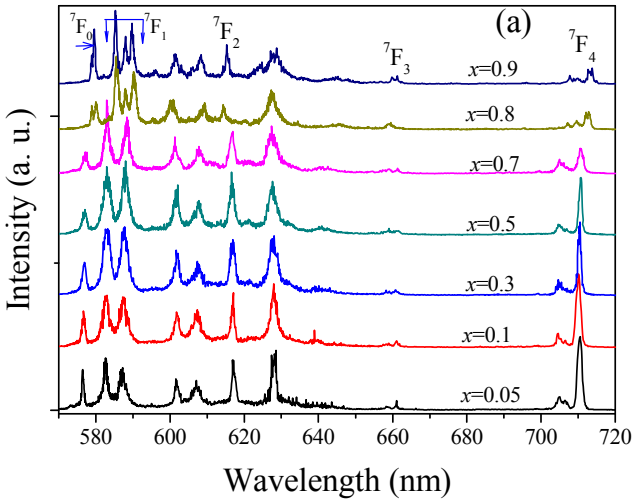

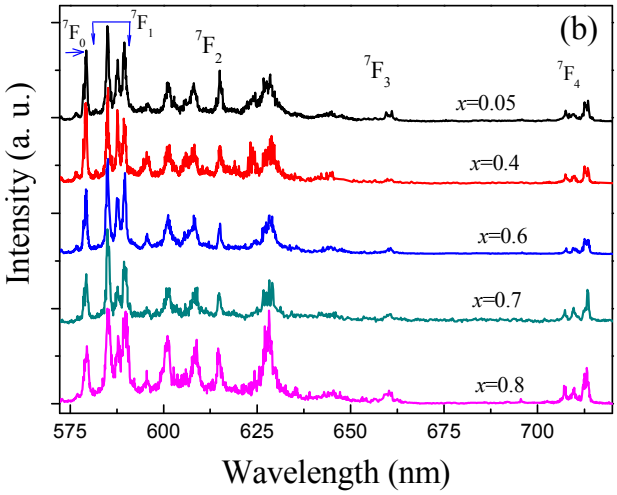

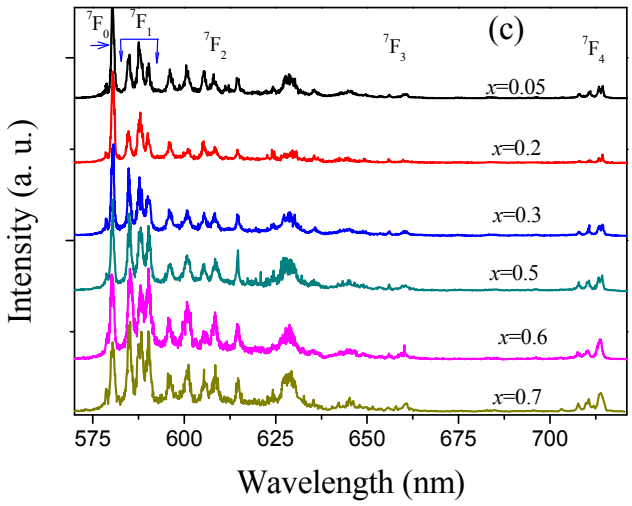

Fig. 11 Color CIE coordinates of R_3SbO_7:xEu^{3+} (R=La, Gd, and Y) calculated from the emission spectra in Fig. 10.

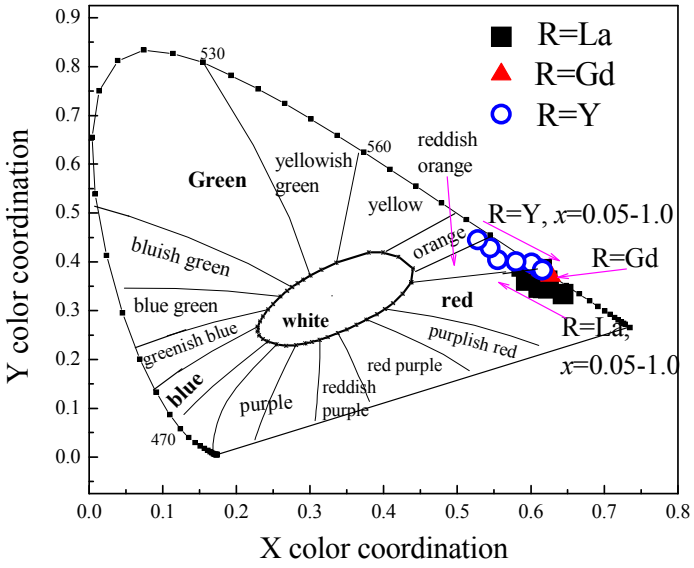

Fig. 12 Luminescence decay curves of $^5D_0$ states in R_3SbO_7:xEu^{3+}, R=La (a), Gd (b), and Y (c) as a function of Eu^{3+} doping concentration. The excitation is using 266 nm Nd:YAG pulsed laser at 300 K.

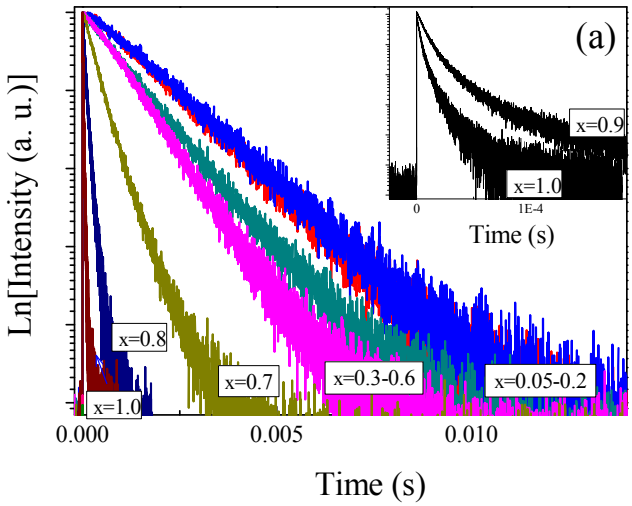

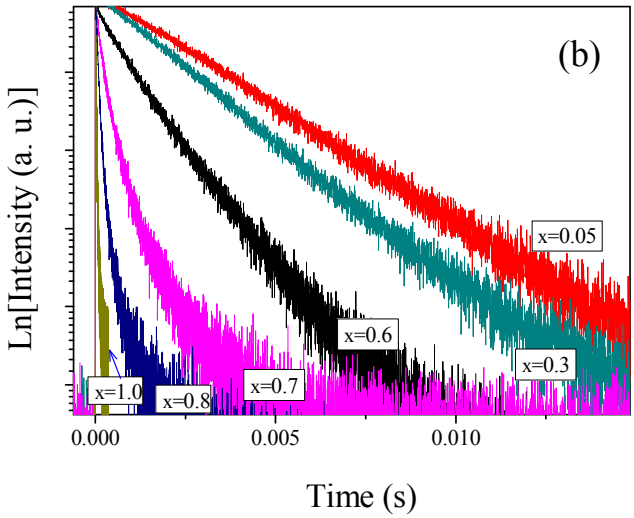

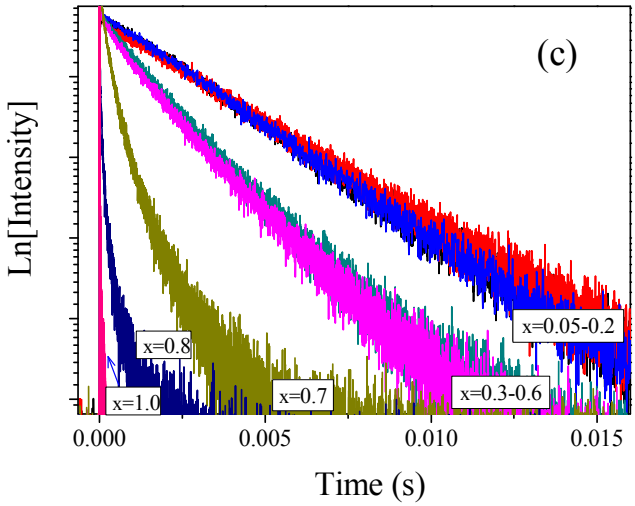

Fig. 13 Luminescence lifetime of $^5D_0$ states of Eu^{3+}-doped R_3SbO_7 (R=La, Gd, and Y) as a function of doping concentration.

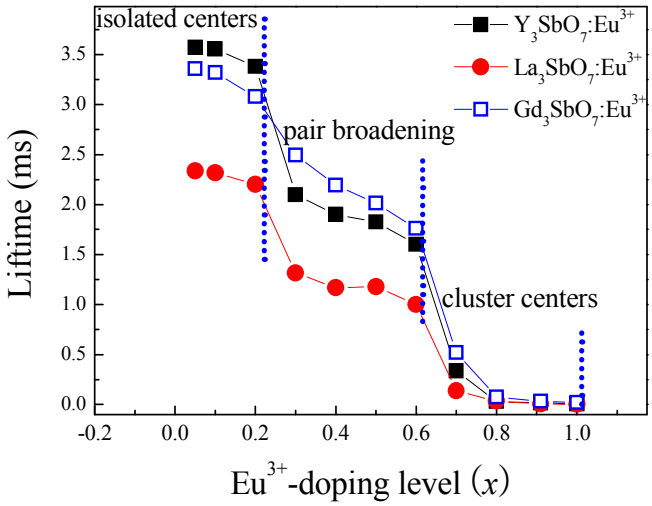

Graphic Abstract

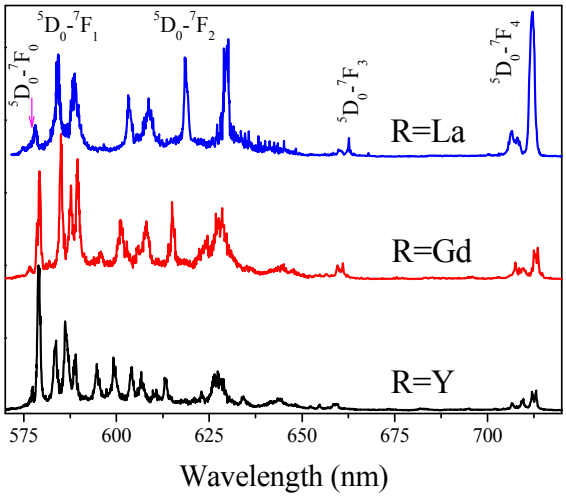

Eu^{3+}-doped antimonates R_3SbO_7 (R=La, Gd, Y) shows distinct luminescence spectra. The $^5D_0 \rightarrow {}^7F_4$ transitions are the dominated emission in Eu^{3+}-doped La_3SbO_7, and Gd_3SbO_7:Eu^{3+} has the strongest emission lines of $^5D_0 \rightarrow {}^7F_1$, while $^5D_0 \rightarrow {}^7F_0$ presents the strongest transition intensity at 580 nm in Eu^{3+}-doped Y_3SbO_7. This is induced by the different microstructures around the surrounding of Eu^{3+} ions in the lattices.